

# CaSAR: Contact-aware Skeletal Action Recognition

Junan Lin<sup>1\*</sup>    Zhichao Sun<sup>1\*</sup>    Enjie Cao<sup>1\*</sup>    Taein Kwon<sup>1</sup>  
Mahdi Rad<sup>2</sup>    Marc Pollefeys<sup>1,2</sup>

<sup>1</sup>ETH Zürich    <sup>2</sup>Microsoft MR & AI Lab, Zürich

## Abstract

*Skeletal Action recognition from an egocentric view is important for applications such as interfaces in AR/VR glasses and human-robot interaction, where the device has limited resources. Most of the existing skeletal action recognition approaches use 3D coordinates of hand joints and 8-corner rectangular bounding boxes of objects as inputs, but they do not capture how the hands and objects interact with each other within the spatial context. In this paper, we present a new framework called Contact-aware Skeletal Action Recognition (CaSAR). It uses novel representations of hand-object interaction that encompass spatial information: 1) contact points where the hand joints meet the objects, 2) distant points where the hand joints are far away from the object and nearly not involved in the current action. Our framework is able to learn how the hands touch or stay away from the objects for each frame of the action sequence, and use this information to predict the action class. We demonstrate that our approach achieves the state-of-the-art accuracy of 91.3% and 98.4% on two public datasets, H2O and FPHA, respectively.*

## 1. Introduction

Action recognition from an egocentric view has become increasingly important in recent years, particularly for real-world applications where hands interact with an object, such as interfaces in augmented reality and virtual reality and human-robot interaction, [9, 24, 28]. Light-weight methods and accurate recognition of the actions are critical for providing a seamless and intuitive user experience. However, existing light-weight egocentric action recognition, such as skeletal action recognition, approaches have limitations due to missing hand-object relation in the existing representation of the hands and objects [4, 26, 28]. These methods mostly use 3D coordinates of hand joints and 8-corner rectangular bounding box of objects as inputs [20, 31], which

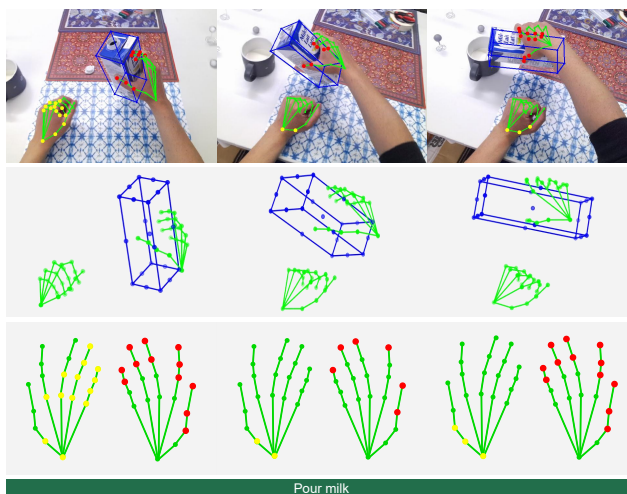


Figure 1. **Action Recognition Using 3D Hand and Object Pose Representations.** We propose Contact-aware Skeletal Action Recognition (CaSAR): a new framework for skeletal action recognition using a novel 3D hands and object poses representation, which includes hand joints positions (green), object 8-corner bounding box (blue), as well as contact points (red) and distant points (yellow) as interaction information. (Row 1) Image frame, (Row 2) Input skeleton frame, (Row 3) Contact points and distant points, (Row 4) Estimated action classes.

do not consider the interaction information between hands and the object. This lack of information can result in inaccurate results, and therefore, will not be practical for the real-world scenarios.

Very recently, [6] illustrated that having the explicit relational information between hands and objects provides a strong cue for the recognition task. To obtain this explicit information, they propose to compute contact maps between hands and object meshes, given 3D hands and object poses. This, however, heavily relies on having accurate and complete mesh models of the hands and the objects, which can be impractical for all possible objects of interest. To address this issue, we propose a novel skeletal action recognition approach called Contact-aware Skeletal

\*Co-first authors

Action Recognition (CaSAR). The key idea is to enforce the network to learn the hands-object interaction information, contact-map, given only hand joint positions and object 8-corner bounding box for each frame of the action sequence. Then, the model learns to predict the action class of the corresponding sequence based on hands and object poses as well as the predicted contact-map, as shown in Figure 1. Our contact-map representation not only encompasses the contact points where hand joints are in direct contact with the object, but also includes distant points for joints located beyond a specified threshold to the object, as illustrated in Figure 1. By incorporating this additional distant information, our method demonstrates even further improvements in accuracy, as the network gains a better understanding of spatial relations between the hands and the object, resulting in enhanced performance on the given task. Moreover, our proposed contact-aware approach does not require additional ground-truth contact information, nor hand and object meshes at inference time. To evaluate the performance of our proposed method, we conducted experiments on two public datasets of H2O [20] and FPFA [14]. Our experiments show that our proposed contact-aware approach achieves state-of-the-art accuracy of 91.3% and 98.4%, on H2O and FPFA, respectively. These results demonstrate the effectiveness of our proposed approach in improving the accuracy of egocentric action recognition.

The contributions of this paper are as follows. First, we propose a novel contact-aware skeletal action recognition framework, CaSAR, that can learn hands-object spatial relations explicitly from hand joints and object bounding boxes as well as geometric shapes implicitly, which removes the need of 3D meshes during the testing time. As a result, our method can adapt to in-the-wild applications. Second, we introduce a novel concept, contact-map, which can model hand-object spatial relations explicitly by setting contact points where the hand joints meet the objects and distant points where the hand joints are far away from the object. Moreover, learning contact-map leads to significant improvement in the accuracy for the task of action recognition. Third, we conduct experiments on two public datasets to evaluate the performance of our proposed method, and achieve state-of-the-art accuracy on both datasets. Overall, our proposed method has significant potential for improving the accuracy of egocentric action recognition and also making the action recognition model understand contact and distant information, which could have important implications for a wide range of real-world applications, including human-computer interaction, augmented reality, and virtual reality.

## 2. Related Work

In this section, we focus on the following research areas closely related to our work: 1) hand-object interaction

recognition, 2) skeletal action recognition, and 3) hand-object contact relation.

### 2.1. Hand-object Interaction Recognition

General action recognition is mainly performed by convolution-based and transformer-based neural networks, which extract RGB-based features. Some examples include I3D [5], SlowFast [12] and Two-stream [30]. In terms of hand-object interaction, earlier works on the hand-object interaction recognition task [1, 10, 11, 25] extracted similar appearance features to recognize the hand-object interaction in the egocentric viewpoint. Recently, Garcia-Hernando et al. [14] showed that hand poses are more helpful than RGB images in recognizing hand actions. Tekin et al. [31], Kwon et al. [20], and Cho et al. [6] proposed each unified framework that performs pose estimation of hands and objects and the hand-object interaction recognition via Long Short-Term Memory (LSTM) [17], Graph Convolutional Network (GCN) [19], and Transformer [32], respectively. In our paper, we present a simple but effective Multilayer Perceptron (MLP) [16] framework with contact context for the same task.

### 2.2. Skeletal Action Recognition

Skeletal action recognition models have been extensively developed nowadays thanks to recent datasets such as NTU120 [23] and H2O [20] that include human skeletons. Some popular model structures are recurrent neural network (RNN) [29] and GCN. Du et al. proposed hierarchical RNN [8], which divides human skeleton into five parts and trains five sub-RNNs for action recognition. Li et al. introduced AS-GCN [21], which extracts implicit relations among joints to improve the performance of traditional GCN which only makes use of fixed skeleton graphs. Zhang et al. came up with Semantics-Guided Neural Networks (SGN) [36], which combines GCN and convolution neural network (CNN) [13] and introduces high-level semantics of joints to enhance the feature representation capability. While skeleton-based action recognition has been extensively researched, little focus has been paid to skeletal hand-object interaction recognition, in which the object and the interaction between hands and the object play a significant role. In our paper, hand-object interaction is tailored for this skeletal action recognition.

### 2.3. Hand-object Contact Relation

In the realm of action recognition, hand-object contact relations emerged as a powerful tool for encoding dynamic interactions. Brahmabhatt et al. [2] proposed to use thermal cameras to capture the hand-object contact maps, reflecting the commonly contacted regions of the object following the grasping action. They additionally presented ContactPose [3], one of the first datasets that combine hand-

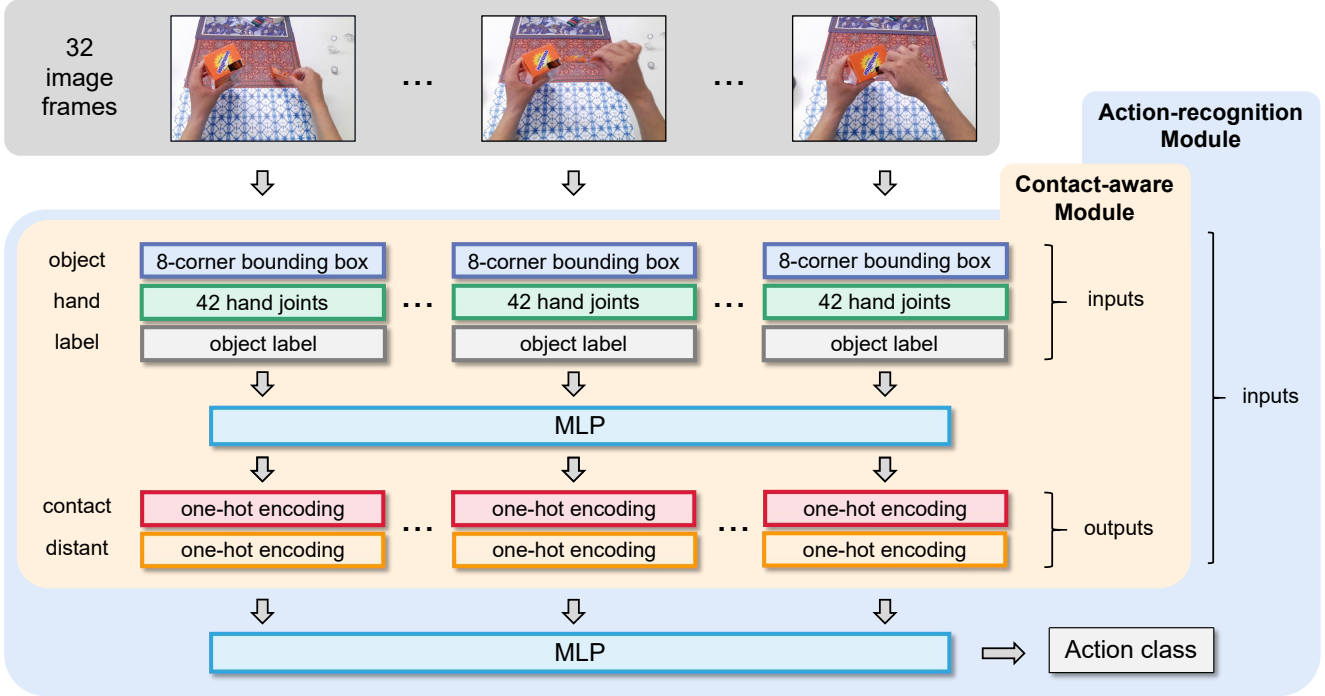


Figure 2. The overall architecture of CaSAR model. We choose 32 as the number of extracted frames for each video segment. For each frame, in addition to the 8-corner bounding box as object pose representation and 42 hand joints as hand pose representation, we further integrate a 42-element one-hot encoding vector that encapsulates contact information and another 42-element one-hot encoding vector indicating distant information, which allows the model to incorporate critical spatial interaction.

object contact information with hand pose, object pose, and RGB-D images. Very recently, Cho et al. [6] also combined contact relations which encode the interaction between two hands and the object into their Transformer-based Unified Recognition module. Unlike the previous work, our framework considers both contact and distant information, which makes the network learn 3D geometric information and leads to better action recognition performance.

### 3. Method

In our work, we first define a novel concept of contact-map, which includes contact points and distant points. We then introduce our framework as illustrated in Figure 2, CaSAR, which leverages the 3D spatial information that is explicitly provided for the task of skeletal action recognition. In this work, we provide contact-map as 3D context. We describe each part in this section.

#### 3.1. Contact-map

Contact-map encompasses spatial information as it consists of contact points, where the hand joints meet the objects, together with distant points, where the hand joints are far away from the objects. The literature has discussed the importance of contact points in hand-object interaction [6] to some extent, but there has been little attention given to

the role of distant points. As we show in our experiment section and the ablation study, our novel formulation of contact-map for hand-object interaction that also focuses on the significance of distant points performs better compared to contact points only. Figure 3 illustrates contact and distant points.

**Contact Points.** We categorize each hand joint as a contact point if it is in contact with the object mesh. In practice, a joint is considered as a contact point if its Euclidean distance to the closest object mesh vertex is less than a threshold  $\eta_c$ . In our experiments, we use  $\eta_c = 2\text{ cm}$ , which is an optimal value considering the object dimension and sparsity of the object mesh.

**Distant Points.** A hand joint is categorized as a distant point if its Euclidean distance to the closest object mesh vertex surpasses a threshold of  $\eta_d$ . In our experiments, we use  $\eta_d = 20\text{ cm}$  for the H2O dataset and  $\eta_d = 10\text{ cm}$  for the FPHA dataset considering their hand movement distribution, which helps to obscure the joints that have little interaction to the object.

#### 3.2. CaSAR

Skeletal action recognition methods aim to understand and classify human hand-object interaction actions from 3D



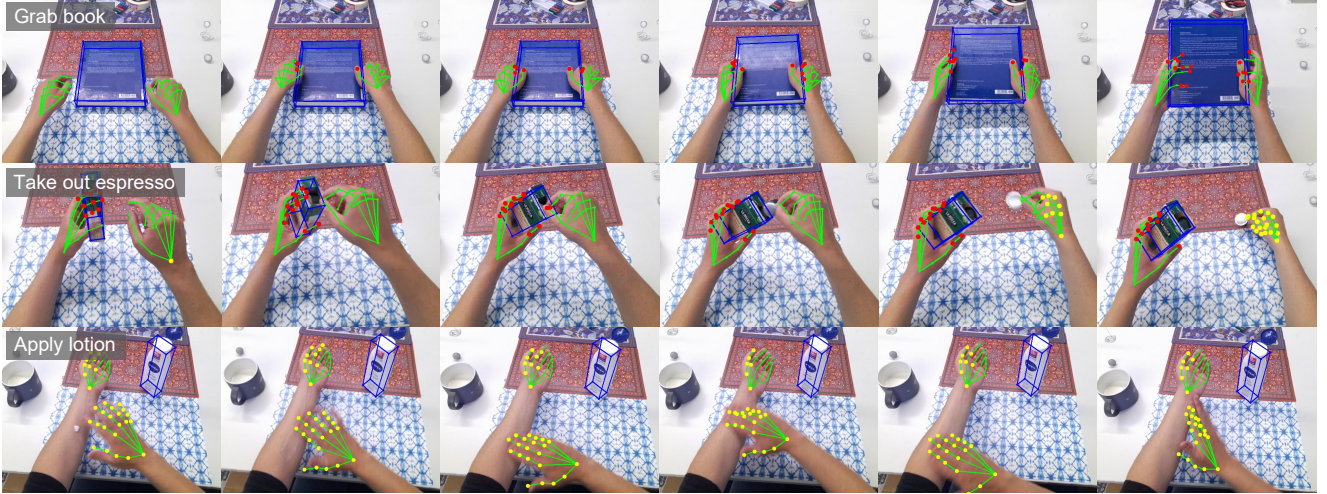


Figure 3. Examples of Contact points (red) that are closer than 2 cm to the object and distant points (yellow) that are more than 20 cm away from the object on the H2O dataset.

hand and 3D object pose. In this work, we propose to leverage 3D spatial context in addition to the skeleton data. We use contact and distant points as the context.

Let  $\mathcal{T} = \{(x_1, y_1), (x_2, y_2), \dots, (x_n, y_n)\}$  be the skeleton training set. In this set, each  $x_i$  is composed of  $N_f$  frames of the following parts: a sequence of 3D coordinates of 21 hand joints on both hands denoted as  $\mathbf{h}_j \in \mathbb{R}^{3 \times 21 \times 2}$ , a sequence of 3D object poses represented by 3D coordinates of 21 points on an 8-corner bounding box denoted as  $\mathbf{o}_j \in \mathbb{R}^{3 \times 21}$ , and a sequence of object label represented using an 8-element one-hot encoding vector denoted as  $\mathbf{l}_j \in \mathbb{R}^8$ , in which  $j = 1, 2, \dots, N_f$ . The corresponding action label is denoted as  $y_i$ . Each  $x_i \in \mathbb{R}^{N_f \times 197}$  is represented as:

$$x_i = \underbrace{\mathbf{h}_1 \mathbf{o}_1 \mathbf{l}_1}_{\text{hand, object, object label}} \dots \underbrace{\mathbf{h}_{N_f} \mathbf{o}_{N_f} \mathbf{l}_{N_f}}_{\text{hand, object, object label}}$$

where  $N_f = 32$  is the total number of frames per action. Notice that  $\mathbf{l}_1 = \mathbf{l}_2 = \dots = \mathbf{l}_{N_f}$ , as the object label remains the same within the same action.

We train the Action Recognition network denoted as  $g$  on the skeleton training set  $\mathcal{T}$ , where the input is concatenated with the contact-map predicted by network  $f$ . Network  $f$  is trained on a contact training set  $\mathcal{T}^c = \{(p_1, q_1), (p_2, q_2), \dots, (p_m, q_m)\}$ , where  $p_i = [\mathbf{h}_i, \mathbf{o}_i, \mathbf{l}_i] \in \mathbb{R}^{197}$  consists of 3D hand joints, 3D object pose, and object label, and  $q_i = [\mathbf{c}_i, \mathbf{d}_i] \in \mathbb{N}^{84}$  represents contact points  $\mathbf{c} \in \mathbb{N}^{42}$  and distant points  $\mathbf{d} \in \mathbb{N}^{42}$  of both left and right hands.  $i$  denotes the  $i$ -th sample in the dataset. **Loss.** We optimize the following objective function over  $\theta_f$  and  $\theta_g$ , the parameters of networks  $f$  and  $g$  as follows:

$$\mathcal{L}(\theta_g, \theta_f; \mathcal{T}, \mathcal{T}^c) = \mathcal{L}_{\text{contact}} + \lambda \mathcal{L}_{\text{action}} \quad (1)$$

Where  $\lambda$  is a hyperparameter that controls the balance between the action recognition and contact map prediction objectives.  $\mathcal{L}_{\text{action}}$  is cross-entropy action recognition loss associated with network  $g$ :

$$\mathcal{L}_{\text{action}} = -\frac{1}{n} \sum_{(x_i, y_i) \in \mathcal{T}} \sum_{c=1}^C y_{i,c} \cdot \log(g([x_i, f(x_i; \theta_f)]_c; \theta_g)) \quad (2)$$

where  $y_{i,c}$  is the indicator function that equals 1 if sample  $i$  belongs to class  $c$ , otherwise 0.  $g(\cdot)_c$  is the predicted probability that sample  $i$  belongs to class  $c$ , and  $C$  is total number of action classes.

$\mathcal{L}_{\text{contact}}$  is the contact-map prediction loss associated with network  $f$ . As in practice, the contact-map contains imbalanced class distribution between contact points and non-contact points, and distant points and non-distant points; we use Focal Loss [22] for  $\mathcal{L}_{\text{contact}}$ :

$$\mathcal{L}_{\text{contact}} = -\frac{1}{m} \sum_{(p_i, q_i) \in \mathcal{T}^c} \alpha q_i \cdot (1 - \hat{q}_i)^\gamma \cdot \log(\hat{q}_i) + (1 - \alpha)(1 - q_i) \cdot (\hat{q}_i)^\gamma \cdot \log(1 - \hat{q}_i) \quad (3)$$

where  $\hat{q}_i = h(p_i; \theta_h)$  is the predicted probability of the positive class for sample  $i$ . In our experiments, we use  $\alpha = 0.5$  and  $\gamma = 4$ .

## 4. Experiments

In this section, we present and discuss the results of our evaluation on two public datasets. We first describe the datasets and the implementation details. Then, we evaluate our method and compare it to the state-of-the-art as well as the results of an ablative analysis of our method.

## 4.1. Datasets

We train and evaluate our proposed approach on H2O [20] and FPFA [14].

**The H2O Dataset.** H2O dataset [20] is acquired in indoor settings in which the subjects interact with objects using both of their hands. It includes more than 570K RGB-D frames and 933 trimmed action clips. The dataset features 36 distinct action classes, which are combinations of 8 object classes and 11 verb classes. The dataset also includes annotated accurate ground-truth data for left and right hand pose, 6D object pose, camera pose, object labels, action labels, and object meshes, with which we can derive ground-truth contact and distant points for the training of the contact-aware module.

**The FPFA Dataset.** FPFA dataset [14] studies the use of 3D hand poses of only one hand to recognize first-person dynamic hand actions interacting with 3D objects. It includes RGB-D video sequences comprised of more than 100K frames of 45 daily hand action categories, involving 26 different objects in several hand configurations. The dataset also includes annotated accurate ground-truth data for right hand pose, 6D object pose, viewpoints, object labels, action labels, and object meshes. However, 6D object pose and object meshes are only available in 4 objects related to 10 action classes in this dataset, and therefore, we use the subset where these data exist for training and testing, following [6, 31].

Note that due to the size of the dataset and the availability of two hands, we decide to set up our experiment mainly on the H2O dataset. By following this, for the simplicity of illustration, the dimensions of variables above and in the below subsections are only for the H2O dataset, adjustments should be made to adapt to FPFA or other datasets.

## 4.2. Implementation Details

As we show in our ablation study, we employ MLP-based networks for both networks  $f$  and  $g$  described in Section 3.2. Both of them have 2 hidden layers, with ReLU being the activation function for hidden layers and Sigmoid being the activation function for the last layer. The number of nodes in each hidden layer is 256, 5000 for  $f$  and  $g$ , respectively. Note that the input,  $x_i$ , is flattened before feeding into the networks.

In practice, we first train the contact-aware module  $f$  by setting  $\lambda = 0$  and then freeze its weight to predict the action recognition module  $g$ . The reason is that the train set  $\mathcal{T}^C$  does not require action labels, therefore, the network  $f$  can be trained on more samples. In addition, it removes the need of tuning the hyperparameter  $\lambda$  in Eq. 1. The model is trained with the Adam optimizer [18] with the learning rate schedule that follows a step-wise decay strategy. Specifically, we start with  $1 \times 10^{-4}$ , and every 20 epoch we reduce

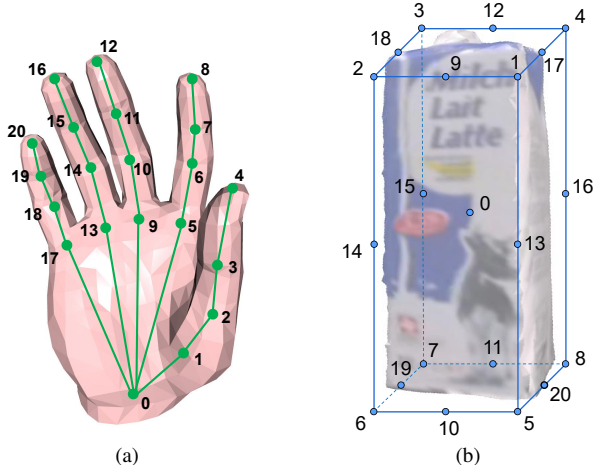


Figure 4. Model and enumerated points for (a) hand and joints, (b) 8-corner bounding box.

it by 30% and train for a total number of 100 epochs. We train the network  $g$  for 600 epochs, with the initial learning rate starting at  $1 \times 10^{-5}$  and we reduce it by 30% for every 200 epochs.

**Uniform frame length.** The length of the frames for each action exhibits considerable variability. To match the input size of the networks, it is necessary to standardize the frame length across all actions. Empirically, we set a uniform length of  $N_f = 32$  frames as we observed this number as the optimal number of frames to extract the requisite information. When we encounter video segments exceeding the length, we select  $N_f$  frames uniformly from the original video. For video segments shorter than this length, we use a repeat strategy to duplicate frames to pad it up to the total length, which works best in our case. We also tried different strategies, such as zero padding, but did not bring improvement compared to the current strategy.

**Hand pose annotation.** H2O [20] dataset provides MANO [28] hand fits for both left and right hand, as shown in Figure 4a. The order of the joints is fixed. In each frame, the 3D coordinates of the 42 joints of two hands are also given; we conclude them in the vector  $h$  as follows:

$$\mathbf{h} = [\mathbf{h}^{\text{Left}}, \mathbf{h}^{\text{Right}}] \subset \mathbb{R}^{126} \quad (4)$$

Where  $\mathbf{h}^{\text{Left}}, \mathbf{h}^{\text{Right}} \subset \mathbb{R}^{63}$  denote the 3D coordinates of 21 joints on the left and right hands.

**Object pose annotation.** H2O [20] dataset provides high-quality object meshes. With the provided  $4 \times 4$  homogeneous transformation matrix in each frame, we can obtain the position of the object at the corresponding moment. Additionally, the label of the object, and the 3D coordinates of

21 points (1 centre, 8 corners, 12 mid-edge points, as illustrated in Figure 4b) of the 8-corner bounding box in each frame are also included in the dataset. The order of the points is fixed. We conclude them in the object label vector  $\mathbf{l} \subset \mathbb{R}^8$  and the object pose vector  $\mathbf{o} \subset \mathbb{R}^{63}$ .

### 4.3. Comparison Framework

**Comparison to State-of-the-Art Baselines** We compare our skeletal action recognition result to the state-of-the-art methods in Table 1. With 8-corner bounding boxes as object pose representation, 3D coordinates of joints as hand pose representation, and contact points and distant points as additional input features, our CaSAR model achieves an accuracy of 91.3% and 98.4% on top-1 action class that matches the object class, which are the best accuracy among SOTA methods on the H2O, and FPFA datasets, respectively. It is notable that, in contrast to H2OTR [6] that relies on object meshes, ours does not require mesh at inference time.

Model	Modality	H2O	FPFA
		Acc.(%)	Acc.(%)
C2D [33]	RGB	70.7	-
I3D [5]	RGB	75.2	-
SlowFast [12]	RGB	77.7	-
Tekin et al. [31]	RGB	68.9	97.0
TA-GCN [20]	*Skeleton	79.3	-
Wen et al. [35]	RGB	86.4	-
H2OTR [6]	*Skeleton+contact	90.9	<b>98.4</b>
<b>Ours</b>	Skeleton+contact	<b>91.3</b>	<b>98.4</b>

Table 1. Comparison to state-of-the-art methods for action recognition on test sets of H2O and FPFA. Note that our method uses ground-truth skeleton information directly from the H2O and FPFA datasets. \* indicates predicted skeletons.

**Qualitative and Quantitative Results** In Figure 5, we show the confusion matrix for the ground truth and predicted action labels. While our model achieves high accuracy in distinguishing among different classes, the prediction accuracy of Chips related actions is lower than other classes. This can be explained by the lower accuracy of contact point prediction of the object Chips as shown in Table 2. Also, the misclassification of the “*spray Spray*” action is related to the low distant point prediction accuracy of the object Spray. Figure 6 and 7 show qualitative results on both success and failure cases of our proposed approach on the H2O and FPFA datasets, respectively.

**Contact-map evaluation.** Table 2 shows the prediction accuracy of contact-aware module  $f$ , including both contact and distant points, for different objects. We can ob-

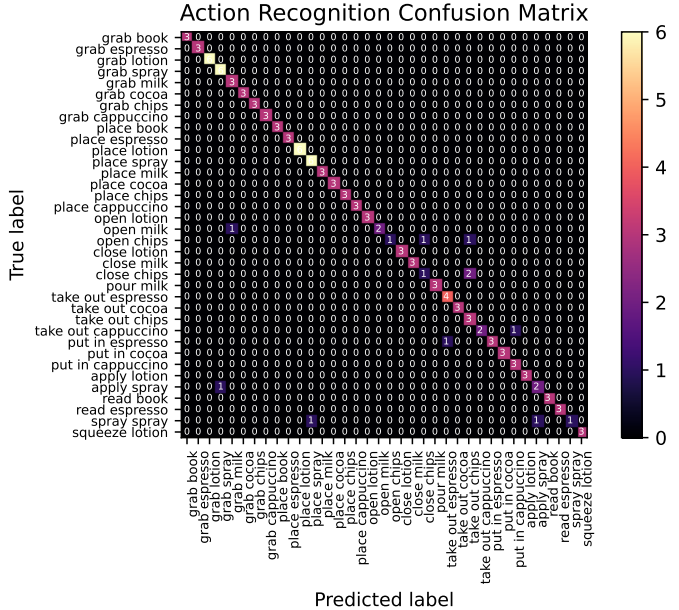


Figure 5. Confusion matrix for action recognition of H2O.

serve that predicting distant points is more accurate on average. This is expected as contact points have much harder constraints to be predicted compared to distant points. Upon analyzing individual objects closely, we observe that the accuracy of predicting contact points varies across different object types. Particularly, the highest accuracy in contact point prediction is attained for objects labeled as Book, Espresso, Cocoa, and Cappuccino, while this precision diminishes for the Chips object, which possesses a cylindrical shape. This discrepancy in accuracy could be attributed to the distinct shapes of these objects. Objects that exhibit cube-like geometries align closely with the concept of an 8-corner bounding box, thereby facilitating accurate contact point estimation. Conversely, the Chips object’s cylindrical form complicates the process of deriving contact maps from an 8-corner bounding box representation. Furthermore, the Chips object involves actions like “*take out Chips*”, wherein a substantial part of the hand penetrates the object’s interior. This contrasts with interactions concerning other objects, primarily occurring on the object’s surface. Consequently, predicting contact points for the Chips object becomes more challenging. Figure 8 shows some examples of the predicted contact-map.

### 4.4. Ablation Study

We discuss here the results of experiments we perform using H2O to describe better our method.

**Baselines.** We introduce two baseline network architectures in our study. Firstly, we incorporate LSTM [17] as a baseline model due to its established efficacy in handling sequential data, demonstrated in domains like action



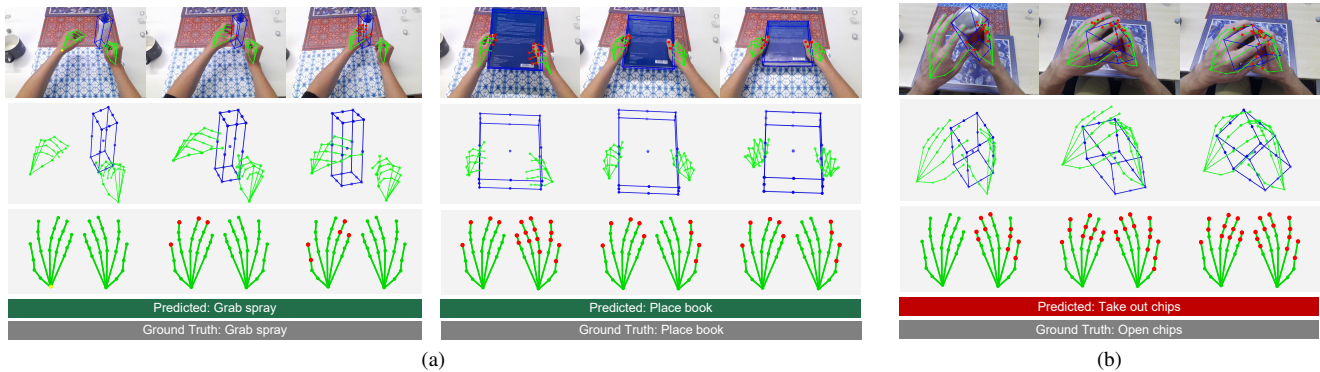


Figure 6. Examples of success cases (a) and a failure case (b) of action recognition on the H2O dataset predicted by our CaSAR. (Row 1) Image frame, (Row 2) Input skeleton frame, (Row 3) Contact map and distant map, (Row 4) Estimated action classes, (Row 5) Ground truth action classes.

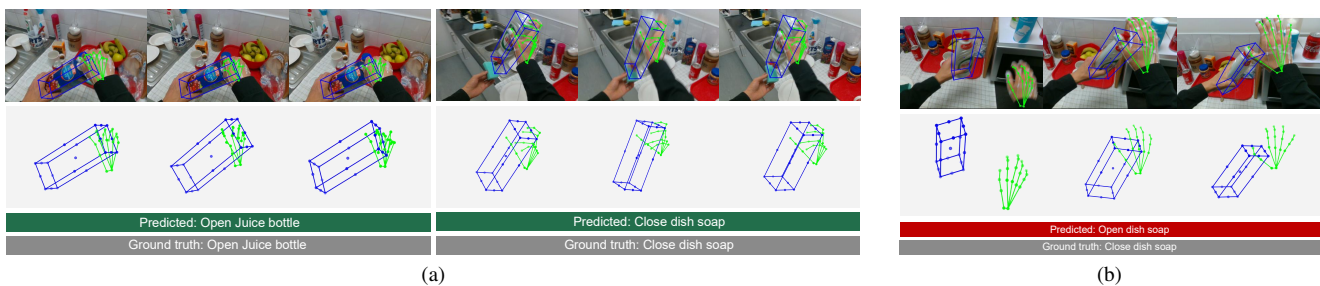


Figure 7. Examples of success cases (a) and a failure case (b) of action recognition on the FPFA dataset predicted by our method, CaSAR. (Row 1) Image frame, (Row 2) Input skeleton frame, (Row 3) Estimated action classes, (Row 4) Ground truth action classes.

Object	Contact acc. (%)	Distant acc. (%)
Book	92.0	99.8
Espresso	94.1	98.9
Lotion	90.1	91.4
Spray	90.8	90.9
Milk	90.0	98.1
Cocoa	95.1	98.3
Chips	83.5	99.4
Cappuccino	91.9	99.8
Average	90.8	96.3

Table 2. Contact-map prediction. We categorize each contact point and distant point prediction accuracy by objects. `Book` achieves the highest in both contact and distance accuracy, whereas `Chips` produces the lowest contact accuracy and `Spray` produces the lowest distance accuracy.

recognition [14]. Secondly, we employ MLP [16] as the other baseline. The comparison between the vanilla MLP and LSTM models is shown in Table 3. Particularly, the

Model	Obj repre.	Contact p.	Distant p.	Acc. (%)
LSTM baseline	bbox	.	.	72.3
MLP baseline	Poisson	.	.	79.8
	bbox	.	.	84.7
CaSAR	bbox	✓	.	90.1
	bbox	.	✓	84.7
	bbox	✓	✓	<b>91.3</b>

Table 3. Ablation study. We run two baselines, LSTM and MLP, as well as different object representations Poisson sampling and bounding boxes to understand better representation for our task. Then, we ablate contact-map to know the effectiveness of constant points and distant points for action recognition. Note that we set up the ablation study on the H2O dataset.

MLP model demonstrates superior performance to LSTM. This can be attributed to the proficiency of MLPs, as they are generally good at capturing simpler patterns and relationships within data, when the dataset is small. The limited size of the data also makes the task not suitable for more complex network architectures such as Transformers [32]. In addition, LSTM, with its ability to capture long-range dependencies, can sometimes lead to overfitting when applied

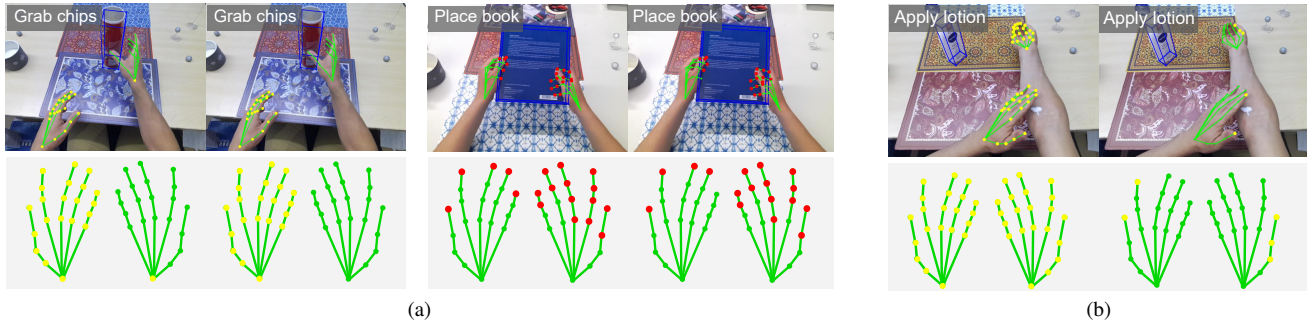


Figure 8. Examples of success cases (a) and a failure case (b) of contact-map and distant map prediction (right), with ground truth (left) on H2O dataset predicted by the contact-aware module of our CaSAR.

to tasks where shorter dependencies are sufficient. To this end, we choose our backbone model as MLP because of its interpretability and the fact that the MLP baseline produces a better result than the LSTM baseline.

**The impact of Contact and Distant Points.** Last rows of Table 3 show the impact of contact-map. Using contact points improves the accuracy significantly by 5.4%, and using distant points brings an additional improvement of 1.2%. Notably, our contact-map module plays a substantial role, accounting for 6.6% of the overall performance improvement. This outcome underscores the critical role that spatial information, in this case, contact-map, plays in enhancing action recognition capabilities.

**Object Representation.** We also evaluate the impact of object representation on the model’s performance. The 8-corner bounding box offers insights into object translation and orientation, yet falls short in providing intricate surface and shape. Object mesh representation, for example, can impart superior geometric insights, which could be potentially essential for understanding hand-object interaction in actions. However, this requires the model to learn an implicit understanding of 3D interaction, which makes the task difficult as it requires a complex model and a large amount of data. We, therefore, conduct a comparative analysis of object representation techniques by providing a subset of object mesh using Poisson sampling. Table 3 confirms that bounding box representation brings a notable 4.9% performance boost in the baseline MLP model.

#### 4.5. Computation Times

We implement our network using PyTorch [27] and the code runs on an Intel i7-12700H CPU with a NVIDIA GeForce RTX 3050 Ti GPU. It takes 25 ms for the contact-map and action recognition at inference time for each action.

## 5. Conclusions

In this paper, we propose a contact-aware action recognition framework, CaSAR, that can predict hand-object contact relations which does not require 3D meshes of the object during the testing time. The framework can learn contact relations explicitly from hand joints and object bounding boxes and geometric shapes implicitly. We further propose a novel concept, contact-map consisting of contact points and distant points, that can significantly improve the performance of action recognition.

To calculate contact maps, our method relies on hand poses and object poses from the datasets. Wrong calculation of contact-map will result in inaccuracies in contact-map prediction action recognition. Also, current datasets with ground truth 3D hand pose and 6D object pose are limited in size compared to large-scale egocentric video datasets such as Ego4D [15], HoloAssist [34], and EpicKitchen [7]. It would be interesting to collect a large-scale dataset to obtain more generalized contact-map. End-to-end action recognition by estimating hand poses, object poses and contact-map from RGB images directly would also be an interesting future direction.

## References

- [1] Sven Bambach, Stefan Lee, David J. Crandall, and Chen Yu. Lending a hand: Detecting hands and recognizing activities in complex egocentric interactions. In *Proceedings of the IEEE International Conference on Computer Vision (ICCV)*, 2015. 2
- [2] Samarth Brahmabhatt, Cusuh Ham, Charles C. Kemp, and James Hays. ContactDB: Analyzing and Predicting Grasp Contact via Thermal Imaging. 2
- [3] Samarth Brahmabhatt, Chengcheng Tang, Christopher D. Twigg, Charles C. Kemp, and James Hays. ContactPose: A Dataset of Grasps with Object Contact and Hand Pose. 2
- [4] Zhe Cao, Gines Martinez, Tomas Simon, Shih-En Wei, and Yaser Sheikh. Openpose: Realtime multi-person 2d pose estimation using part affinity fields. *IEEE Transactions on*



- Pattern Analysis and Machine Intelligence*, PP:1–1, 07 2019. 1
- [5] Joao Carreira and Andrew Zisserman. Quo vadis, action recognition? a new model and the kinetics dataset, 2018. 2, 6
- [6] Hoseong Cho, Chanwoo Kim, Jihyeon Kim, Seongyeon Lee, Elkhan Ismayilzada, and Seungryul Baek. Transformer-based unified recognition of two hands manipulating objects. In *Proceedings of the IEEE/CVF Conference on Computer Vision and Pattern Recognition (CVPR)*, 2023. 1, 2, 3, 5, 6
- [7] Dima Damen, Hazel Doughty, Giovanni Maria Farinella, Sanja Fidler, Antonino Furnari, Evangelos Kazakos, Davide Moltisanti, Jonathan Munro, Toby Perrett, Will Price, and Michael Wray. The epic-kitchens dataset: Collection, challenges and baselines. *IEEE Transactions on Pattern Analysis and Machine Intelligence (TPAMI)*, 43(11):4125–4141, 2021. 8
- [8] Yong Du, Wei Wang, and Liang Wang. Hierarchical recurrent neural network for skeleton based action recognition. In *Proceedings of the IEEE Conference on Computer Vision and Pattern Recognition (CVPR)*, 2015. 2
- [9] Abassin Sourou Fangbemi, Bin Liu, Neng Hai Yu, and Yanxiang Zhang. Efficient human action recognition interface for augmented and virtual reality applications based on binary descriptor. In Lucio Tommaso De Paolis and Patrick Bourdot, editors, *Augmented Reality, Virtual Reality, and Computer Graphics*, pages 252–260, Cham, 2018. Springer International Publishing. 1
- [10] Alireza Fathi, Ali Farhadi, and James M. Rehg. Understanding egocentric activities. In *2011 International Conference on Computer Vision*, 2011. 2
- [11] Alireza Fathi, Xiaofeng Ren, and James M. Rehg. Learning to recognize objects in egocentric activities. In *CVPR 2011*, 2011. 2
- [12] Christoph Feichtenhofer, Haoqi Fan, Jitendra Malik, and Kaiming He. SlowFast Networks for Video Recognition. In *2019 IEEE/CVF International Conference on Computer Vision (ICCV)*, 2019. 2, 6
- [13] Kuniyuki Fukushima. Neocognitron: A self-organizing neural network model for a mechanism of pattern recognition unaffected by shift in position. *Biological cybernetics*, 1980. 2
- [14] Guillermo Garcia-Hernando, Shanxin Yuan, Seungryul Baek, and Tae-Kyun Kim. First-person hand action benchmark with rgb-d videos and 3d hand pose annotations. In *Proceedings of the IEEE Conference on Computer Vision and Pattern Recognition (CVPR)*, 2018. 2, 5, 7
- [15] Kristen Grauman, Andrew Westbury, Eugene Byrne, Zachary Chavis, Antonino Furnari, Rohit Girdhar, Jackson Hamburger, Hao Jiang, Miao Liu, Xingyu Liu, et al. Ego4d: Around the world in 3,000 hours of egocentric video. In *Proceedings of the IEEE/CVF Conference on Computer Vision and Pattern Recognition*, pages 18995–19012, 2022. 8
- [16] Simon Haykin. *Neural networks: a comprehensive foundation*. Prentice Hall PTR, 1994. 2, 7
- [17] Sepp Hochreiter and Jürgen Schmidhuber. Long short-term memory. *Neural Computation*, 1997. 2, 6
- [18] Diederik P. Kingma and Jimmy Ba. Adam: A Method for Stochastic Optimization, 2017. 5
- [19] Thomas N Kipf and Max Welling. Semi-supervised classification with graph convolutional networks. *arXiv preprint arXiv:1609.02907*, 2016. 2
- [20] Taein Kwon, Bugra Tekin, Jan Stuhmer, Federica Bogo, and Marc Pollefeys. H2O: Two Hands Manipulating Objects for First Person Interaction Recognition, 2021. 1, 2, 5, 6
- [21] Maosen Li, Siheng Chen, Xu Chen, Ya Zhang, Yanfeng Wang, and Qi Tian. Actional-Structural Graph Convolutional Networks for Skeleton-Based Action Recognition. In *2019 IEEE/CVF Conference on Computer Vision and Pattern Recognition (CVPR)*, 2019. 2
- [22] Tsung-Yi Lin, Priya Goyal, Ross Girshick, Kaiming He, and Piotr Dollár. Focal loss for dense object detection. In *Proceedings of the IEEE international conference on computer vision*, pages 2980–2988, 2017. 4
- [23] Jun Liu, Amir Shahroudy, Mauricio Perez, Gang Wang, Ling-Yu Duan, and Alex C Kot. Ntu rgb+d 120: A large-scale benchmark for 3d human activity understanding. *IEEE transactions on pattern analysis and machine intelligence*, 42(10):2684–2701, 2019. 2
- [24] Mengdan Lou, Jieyu Li, Guoxing Wang, and Guanghai He. Ar-c3d: Action recognition accelerator for human-computer interaction on fpga. In *2019 IEEE International Symposium on Circuits and Systems (ISCAS)*, pages 1–4, 2019. 1
- [25] Minghuang Ma, Haoqi Fan, and Kris M. Kitani. Going deeper into first-person activity recognition. In *Proceedings of the IEEE Conference on Computer Vision and Pattern Recognition (CVPR)*, 2016. 2
- [26] Arsalan Mousavian, Dragomir Anguelov, John Flynn, and Jana Kosecka. 3d bounding box estimation using deep learning and geometry. In *Proceedings of the IEEE Conference on Computer Vision and Pattern Recognition (CVPR)*, July 2017. 1
- [27] Adam Paszke, Sam Gross, Francisco Massa, Adam Lerer, James Bradbury, Gregory Chanan, Trevor Killeen, Zeming Lin, Natalia Gimelshein, Luca Antiga, Alban Desmaison, Andreas Kopf, Edward Yang, Zachary DeVito, Martin Raison, Alykhan Tejani, Sasank Chilamkurthy, Benoit Steiner, Lu Fang, Junjie Bai, and Soumith Chintala. PyTorch: An imperative style, high-performance deep learning library. In *Advances in Neural Information Processing Systems*, 2019. 8
- [28] Javier Romero, Dimitrios Tzionas, and Michael J. Black. Embodied hands: Modeling and capturing hands and bodies together. *ACM Transactions on Graphics, (Proc. SIGGRAPH Asia)*, 36(6), Nov. 2017. 1, 5
- [29] David E Rumelhart, Geoffrey E Hinton, and Ronald J Williams. Learning internal representations by error propagation. Technical report, 1985. 2
- [30] Lei Shi, Yifan Zhang, Jian Cheng, and Hanqing Lu. Two-stream adaptive graph convolutional networks for skeleton-based action recognition. In *Proceedings of the IEEE/CVF Conference on Computer Vision and Pattern Recognition (CVPR)*, 2019. 2
- [31] Bugra Tekin, Federica Bogo, and Marc Pollefeys. H+o: Unified egocentric recognition of 3d hand-object poses and

- interactions. In *Proceedings of the IEEE/CVF Conference on Computer Vision and Pattern Recognition (CVPR)*, June 2019. [1](#), [2](#), [5](#), [6](#)
- [32] Ashish Vaswani, Noam Shazeer, Niki Parmar, Jakob Uszkoreit, Llion Jones, Aidan N Gomez, Łukasz Kaiser, and Illia Polosukhin. Attention is all you need. *Advances in neural information processing systems*, 30, 2017. [2](#), [7](#)
- [33] Xiaolong Wang, Ross Girshick, Abhinav Gupta, and Kaiming He. Non-local neural networks, 2018. [6](#)
- [34] Xin Wang, Taein Kwon, Mahdi Rad, Bowen Pan, Ishani Chakraborty, Sean Andrist, Dan Bohus, Ashley Feniello, Bugra Tekin, Felipe Vieira Frujeri, Neel Joshi, and Marc Pollefeys. Holoassist: an egocentric human interaction dataset for interactive ai assistants in the real world. In *Proceedings of the IEEE/CVF International Conference on Computer Vision (ICCV)*, 2023. [8](#)
- [35] Yilin Wen, Hao Pan, Lei Yang, Jia Pan, Taku Komura, and Wenping Wang. Hierarchical temporal transformer for 3d hand pose estimation and action recognition from egocentric rgb videos, 2023. [6](#)
- [36] Pengfei Zhang, Cuiling Lan, Wenjun Zeng, Junliang Xing, Jianru Xue, and Nanning Zheng. Semantics-guided neural networks for efficient skeleton-based human action recognition. In *Proceedings of the IEEE/CVF Conference on Computer Vision and Pattern Recognition (CVPR)*, 2020. [2](#)